

DOI: 10.1002/adfm.200800397

# Light-Emission Performance of Silicon Nanocrystals Deduced from Single Quantum Dot Spectroscopy\*\*

By Jan Valenta, Anna Fucikova, František Vácha, František Adamec, Jana Humpolíčková, Martin Hof, Ivan Pelant, Kateřina Kúsová, Kateřina Dohnalová, and Jan Linnros\*

Spectra of individual silicon nanocrystals within porous Si grains are studied by the wide-field imaging microspectroscopy and their *ON-OFF* blinking is detected by the confocal single-photon-counting microscopy. Observed spectral and blinking properties comprise all features reported before in differently prepared single Si nanocrystals (SiNCs). Former apparently contradictory results are shown to be due to different experimental conditions. When the effect of dark periods (*OFF* switching) is removed the common ultimate photoluminescence properties of SiO<sub>2</sub> passivated SiNCs are found, namely the quantum efficiency (QE) of about 10–20% up to the pumping rate corresponding to one exciton average excitation per quantum dot. At higher pump rates the QE is slowly decreasing as the 0.7th power of excitation. This is most likely due to Auger recombination which, however, seems to be weakened compared with measurements of nanocrystal assemblies. We conclude that SiNCs may be pumped above one exciton occupancy to yield a higher light emission, being advantageous for applications.

## 1. Introduction

Light-emitting silicon nanostructures have attracted considerable attention since the first report on photoluminescence (PL) of porous silicon (PSi) in 1990<sup>[1]</sup> with the motivation to build silicon-based photonics. Various light-emitting silicon nanostructures have been prepared and studied with a wide spectrum of methods. However, neither an efficient and reliable light-emitting diode nor a laser has been demonstrated up to now. Moreover, number of papers

on this subject often present apparently contradictory data and a deep fundamental understanding of the light-emission process is still missing. Clearly, more advanced experimental techniques are needed to elucidate the light emission mechanism which is partly hidden in ensemble measurements due to size dispersion.

Single nanocrystal spectroscopy (SNS), using techniques developed for single molecule studies, has already proven to be very efficient in revealing the fundamental properties of direct band gap semiconductor quantum dots.<sup>[2]</sup> SNS makes it possible not only to overcome the inhomogeneous broadening of ensemble spectra but also reveals new phenomena such as emission intermittency (*ON-OFF* blinking), spectral diffusion, and polarization. The application of SNS to single silicon nanocrystals (SiNCs) is still not fully explored because of technical difficulties of sample preparation and the inherently low emission rate of the S-band luminescence of SiNCs. In the literature, there are reports on SiNCs SNS by only four research groups. The groups of Buratto<sup>[3–5]</sup> and Cichos<sup>[6–9]</sup> investigated grains of porous silicon deposited on substrates from diluted colloidal suspension, the Korgel's group<sup>[10]</sup> reported on the properties of single SiNCs prepared by arrested precipitation in liquid (they observed only fast PL emission that will not be discussed in this paper), and the group of Linnros<sup>[11–15]</sup> investigated SiNCs formed on top of oxidized nanopillars made by electron-beam lithography. Only the last group performed investigations of single SiNCs at cryogenic temperatures down to 35 K,<sup>[14,15]</sup> other reports deal only with room-temperature (RT) experiments which is also the case in this work.

The most significant published observations may be summarized as follows: The Buratto's group reported that only about a few percent of present PSi grains show detectable

[\*] Prof. J. Valenta, and A. Fucikova

Department of Chemical Physics and Optics, Faculty of Mathematics and Physics Charles University, Ke Karlovu 3, 121 16 Prague 2 (Czech Republic)

E-mail: jan.valenta@mff.cuni.cz

Prof. F. Vácha, Dr. F. Adamec

Institute of Physical Biology, University of South Bohemia and Institute of Plant Molecular Biology, Academy of Sciences of the Czech Republic, Budweis (Czech Republic)

Dr. J. Humpolíčková, Prof. M. Hof

J. Heyrovsky Institute of Physical Chemistry of the Academy of Sciences of the Czech Republic, v.v.i., Prague 8 (Czech Republic)

K. Kúsová, Dr. K. Dohnalová, Prof. I. Pelant

Institute of Physics of the Academy of Sciences of the Czech Republic v.v.i., Prague 6 (Czech Republic)

Prof. J. Linnros

Department of Microelectronics and Applied Physics, Royal Institute of Technology Electrum 229, 164 21 Kista-Stockholm (Sweden)

[\*\*] This work was supported by the Czech Ministry of Education, Youth and Sports through the research centers LC510, LC06063 and the research plan MSM0021620835, by the project 202/07/0818 of the GACR, the project IAA101120804 of the GAAV, and the Institutional Research Plan (IP) AV0Z 10100521 and by (JL) the National Swedish Research Council (VR). The authors thank S. Bakardjieva for the HR-TEM measurements.

PL but their quantum efficiency (QE) can be as high as 88%.<sup>[4]</sup> They found the PL spectra of single grains to be broad and sometimes consisting of several narrower (vibronic) bands with full-width at half-maximum (FWHM) of about 115 meV and splitting of about 160 meV (proposed origin due to the stretching vibration of the Si–O–Si bridge bond).<sup>[3]</sup> Cichos and coworkers<sup>[6,8,9]</sup> reported on PL spectra of single PSi or pyrolysis particles (FWHM of about 100 meV or wider) with a low-energy side-band shifted by 120–190 meV in some cases. Observed PL (nonstationary) blinking of PSi grains obeys a power law statistics and it is intensity dependent due to the intensity dependent tunneling rate of the Auger assisted processes. The distribution of *OFF* times is related to the bleaching and recovery of the PL of PSi.<sup>[6]</sup> Finally, the Linnros' group observed that only about a percent of fabricated nanopillars shows detectable PL that can reach QE of up to

35%.<sup>[11]</sup> The PL spectra of single Si quantum dots are always formed by a single band with FWHM mostly about 120 meV.<sup>[11]</sup> PL intermittency indicates blinking between only two states and the *ON* and *OFF*-interval distribution is exponential indicating random switching. The *ON*-time intervals shorten with the square of the excitation power, indicating possible charging by Auger recombination.<sup>[14]</sup>

From the above given summary, it is evident that the published results of single SiNCs studies seem to reveal apparent differences in the behavior of the differently prepared samples. Here, we present the application of wide-field imaging microspectroscopy and confocal, single-photon-counting (SPC) microscopy to study SNS of PSi grains. Our results allow us to unify the view on single SiNCs and to find the limits of the performance of the S-band emission in SiNC/SiO<sub>2</sub> nanostructures.

## 2. Single Particle PL Spectra and Blinking Statistics

In Figure 1, we present a typical PL image of the deposited suspension and the broad PL spectrum of a rather large and brightly emitting spot (apparently containing many luminescing SiNCs and its spectrum resembling the ensemble spectrum) and several PL spectra from weakly emitting diffraction limited spots on the sample surface (Fig. 1c). One can see narrow emission bands peaking at different wavelengths through the whole ensemble PL band. The most frequent PL band is of Gaussian shape with the FWHM around 120 meV as shown by fitting the spectral peaks (yellow lines). Repeated measurements of PL spectra of single PSi grains reveal changes of spectral shapes. To demonstrate this phenomenon we plot in Figures 1d and e sequences of nine consecutive measurements (each acquisition lasts 30 min) of PL spectra from two individual particles. One can see that even for such long acquisition time there is observable *ON–OFF* switching as well as “spectral diffusion” of the order of 100 meV. We have to note that the typical PL band is sometimes asymmetrically broadened to the low-energy side, possibly due to unresolved phonon or vibrational side-bands that become clearly resolved only at stronger pumping.<sup>[3,9,13]</sup>

The temporal variation of the PL intensity is studied using the SPC set-up. Under cw excitation (444 nm) the arrival times of detected photons (events) at two APD detectors are recorded (the detection period

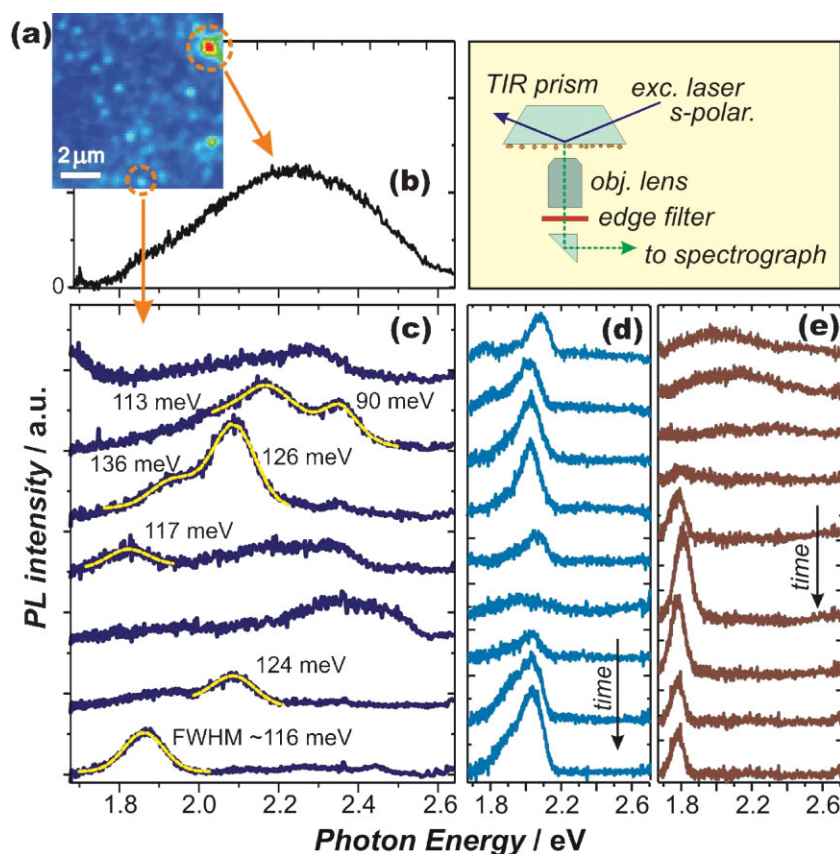


**Figure 1.** Spectral characteristics of single PSi grains. a) PL image (in false colors) of PSi grains deposited on the TIR prism and detected by an imaging spectroscopy set-up in the imaging mode (acquisition time is 3 min). The experimental arrangement is illustrated by the right inset image. Most of the emitting spots have the diffraction limited size with FWHM about 410 nm (its image covers just 3 pixels of the CCD detector). b) The broad PL spectrum of a strongly emitting spot, which consists of many luminescing SiNCs. c) Eight spectra of different diffraction-limited weakly emitting spots measured simultaneously during one 30 min acquisition at different locations on the sample. Some of the PL peaks are fitted with a Gaussian band (yellow lines) with the FWHM indicated. d) and e) Sequences of nine 30 min acquisitions of PL spectra from two different emitting spots demonstrating the *ON–OFF* blinking and spectral diffusion. The time sequence starts at the top of the panels.

is between 5 and 15 min). The detection events are binned per selected time slots and plotted against time. If the selection of the bin length is optimized (here the optimal value is between 0.1 and 0.3 s) the intensity time evolution reveals clear multilevel fluctuations (see Fig. 2a) as documented by constructing an intensity histogram (see Fig. 2b). The most abundant intensity levels are then found by fitting the histogram with several Gaussians and finally the thresholds between emission levels are calculated. For the case given in Figures 2a and b, the intensity peaks of the zero, the first and second states are given in the figure.<sup>[16]</sup> The first level corresponds to the background or OFF state and higher levels are labeled single, double, triple, etc. ON state (see text below). It is interesting to note that Mason et al.<sup>[5]</sup> also observed multilevel blinking of single P*Si* grains and presented multilevel histograms but calculated from PL intensities of many single emitting spots (ensemble averaging) in contrast to our time-averaging of signals from a single spot.

When the proper bin lengths and intensity thresholds are defined, the statistics of dwell times of a blinking particle in each state is calculated. In Figures 2c–e, we plot the distribution of dwell times measured under  $0.6 \text{ kW} \cdot \text{cm}^{-2}$  excitation and using 100 ms bin time. The OFF time distribution experimental points are well fitted by a power law dependence with an exponent around  $-1.38$ . For the single and double ON state, the data follow a power-law dependence  $t^{-1.5}$  at shorter times but then decreases faster following an exponential decay. Therefore, the distribution of ON states on the full experimental time range was fitted with a combination of a power-law and an exponential decay: The characteristic exponential decay time  $\tau$  for the single ON state is about 2.3 s and becomes shorter  $\sim 0.96$  s for the double ON state.

### 3. Discussion

Comparing the present data with literature we conclude that the spectral signature of the S-band emission of a single SiNC at RT is a single Gaussian band with a FWHM around 100–150 meV. It is the same in all types of Si/SiO<sub>2</sub> nanostructures prepared by different methods. In case of the P*Si* grains,

the spectrum may be more complicated consisting of several superimposed PL bands, which can switch ON–OFF. This is because there can be several SiNCs, not a proper single NC, within the optically resolved (diffraction limited) spot. In fact, the probability to break the P*Si* layer into proper individual SiNCs using common separation techniques is low and the clustering may take place also during the colloid deposition on a substrate. In spite of this fact, it is possible to observe optical signatures of single emitting SiNCs within P*Si* clusters, if most of the present SiNCs are in the dark state (OFF period) not participating in emission simultaneously.

The interpretation of the multilevel blinking is based on the fact that Si nanopillars containing a single SiNC showed

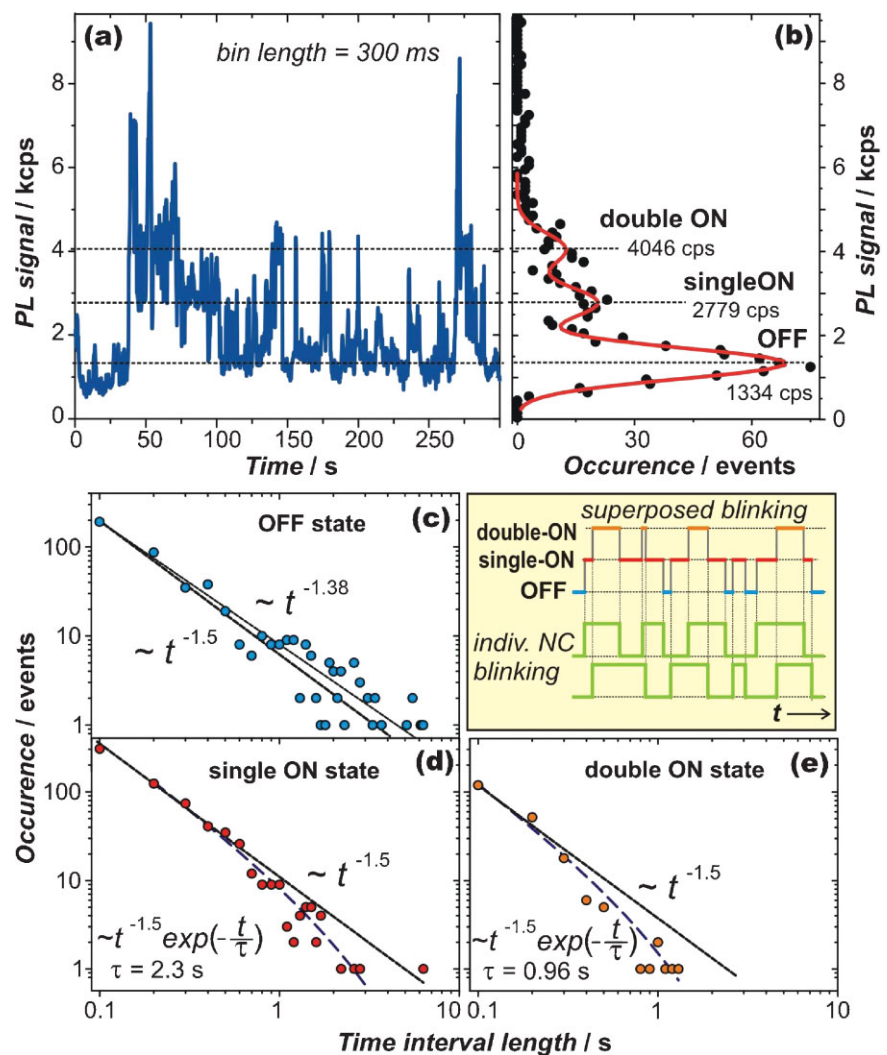


**Figure 2.** Blinking characteristics of single P*Si* grains. a) Typical time trace obtained from a single P*Si* nanoparticle by binning of the photon counting events per 300 ms slots. (The most apparent signal levels are indicated by dashed lines.) b) The occurrence histogram of intensities from the left panel. Red line is a fit with three Gaussian peaks. c–e) Histograms of distribution of dwell times for the OFF state (c), single- (d) and double- (e) ON states ( $0.6 \text{ kW cm}^{-2}$  excitation power and 100 ms bin length). Experimental points are fitted with the power-law dependence (black dashed lines) whose exponents are indicated. In addition, single and double ON state distributions are also fitted with a combination of  $t^{-1.5}$  power-law dependence and an exponential bending tail (blue dashed curves). The inset illustrates the possible superposition of blinking of individual SiNCs producing a multilevel blinking.

exclusively blinking between two states as shown by our previous work.<sup>[14]</sup> We propose that also in the case of a single SiNC in a PSi grain the blinking takes place only between two states and therefore there is only one active luminescence center. Then the multilevel blinking (Fig. 2) is explained as overlapping contributions of two, three or more individual SiNCs emitting simultaneously within an optically resolved spot. We have to note that even such a simple superposition (without any interaction of NCs) affects the statistical distribution of *ON* and *OFF* states as is schematically illustrated in the inset in Figure 2.

Concerning the *ON* and *OFF* interval distributions, the literature data reveal different types of blinking statistics of SiNCs in nanopillar and PSi samples. Namely the distribution of *OFF* and *ON* dwell times was found to be exponential in the nanopillar samples<sup>[14]</sup> (indicating random telegraph switching model<sup>[17]</sup>) while the inverse power-law dependence  $\sim t^{-\alpha}$  (with  $\alpha$  between 1.3 and 2.2) is typical for PSi samples.<sup>[6]</sup> In this work, we present blinking statistics of PSi grains that show both types of statistics: The power-law dependence with  $\alpha$  close to 1.5 or slightly shorter is observed for *OFF* interval distributions and for *ON* distributions at a short time scale (Fig. 2). For longer *ON* dwell times, the distribution becomes exponential (especially for multiplied *ON* states). The same behavior described by Equation 2 was observed also for the nanocrystals of II–VI semiconductors.<sup>[18]</sup> Now the above mentioned discrepancy is easily understood: measurements on single SiNCs in nanopillar samples by Sychugov et al.<sup>[14]</sup> addressed only the long part of the time scale (bin size being 15 s due to a slow detection system and low-emission rate under weak excitation), i.e., the exponential bending tail of the distribution. The theoretical model predicting exactly this kind of blinking distribution in semiconductor quantum dots was developed by Marcus and coworkers.<sup>[19–22]</sup> It is based on the diffusion-controlled electron-transfer (DCET) reaction model in which a diffusive process occurs along free-energy potentials. The DCET model leads to a  $-1.5$  power-law decay for both *ON* and *OFF* statistics as well as the breakdown of the power-law with an exponential tail for the *ON* time distribution and eventually also for the *OFF* time distribution at much longer times. Anomalous diffusion could cause the exponent to deviate from  $-1.5$ .

The optical properties of Si nanocrystalline materials described in the literature are seemingly very sensitive to fabrication conditions. However, when the strong dependence on the experimental conditions (mainly excitation intensity and wavelength) is taken into account the properties reveal clear uniformity, insensitive to the preparation and treatment conditions.<sup>[23]</sup> Here we show that the same is true for the emission of single SiNCs. This fact is markedly illustrated by Figure 3a, where we collected data from all available published works on SNS of SiO<sub>2</sub> passivated SiNCs. The excitation photon rate  $R_{\text{ex}}$  is calculated as a product of excitation intensity (in photons  $\cdot$  s<sup>-1</sup>  $\cdot$  cm<sup>2</sup>) and excitation cross-section  $\sigma$  (in cm<sup>-2</sup>) taken from Kovalev et al.<sup>[24]</sup> The emission photon rate  $R_{\text{em}}$  is the detection rate (in counts per second – cps) of the single *ON* state signal (it means that the effect of dark *OFF* periods is

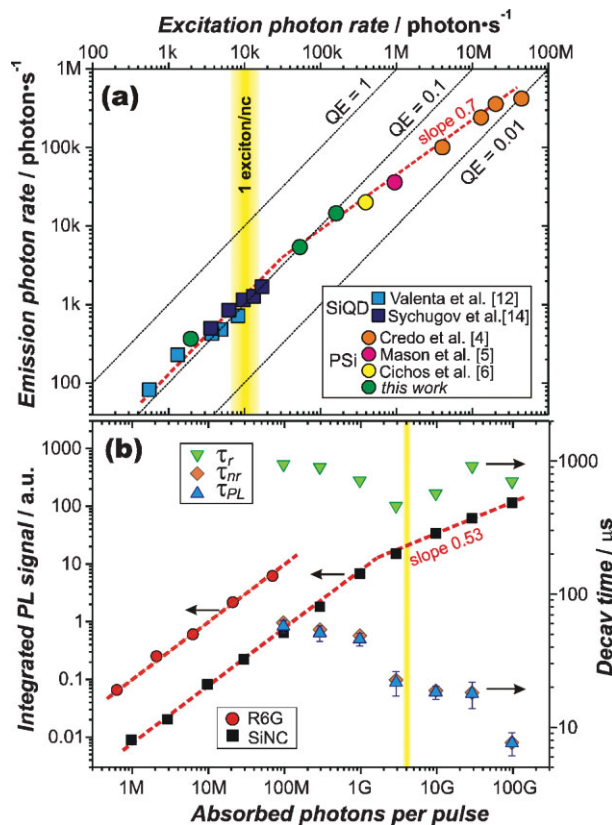


**Figure 3.** Performance of the S-band emission of SiNCs. a) The emission photon rate of the single *ON* state signal as a function of the excitation photon rate. Dotted lines show regions of different PL QE of SiNCs. b) The ensemble PL measurement of SiNC suspension under intense stirring. The integrated PL signal (black rectangles) is compared to integrated signal of reference solution of Rhodamine 6G (red circles). The measured PL decay time and derived radiative and nonradiative lifetimes are plotted by violet triangles, green rectangles, and blue circles, respectively. The yellow vertical line indicates where the average absorption of one photon per nanocrystal per pulse takes place.

excluded) divided by the overall detection efficiency (detected count per emitted photon). Indeed, all data fit in a clear linear/sublinear dependence (in the log–log scale) over almost five orders of magnitude of excitation rate. The emission photon rate increases linearly with the excitation rate up to about 20 kcps and then slightly saturates following roughly a  $R_{\text{em}} \sim R_{\text{ex}}^{0.7}$  dependence for three orders of excitation increase. This indicates that additional nonradiative recombination channels (most probably Auger recombination) reduce the QE from about 0.15 at very low excitation to about 0.01 for the highest excitation. In addition, there is no clear saturation at least up to an excitation rate of  $3 \times 10^7$  photons  $\cdot$  s<sup>-1</sup>. This is surprising because up to now Auger recombination was generally assumed to quench SiNC emission under strong excitation very efficiently.

The break point between linear and sublinear behavior in Figure 3a is supposed to happen when the creation of the second electron-hole pair during the lifetime of the first one becomes probable. As the excited state lifetime of a SiNC is of

the order of  $100 \mu\text{s}$ <sup>[25]</sup> the break point is supposed to be around the excitation rate of  $10^4 \text{ photon} \cdot \text{s}^{-1}$ . The difference between the expected and experimental break point is well within the accuracy of plotted data.

The influence of the PL bleaching due to persistent OFF switching can, in principle, be removed not only by the detection of ON state level of a single SiNC but also by fast circulation of the sample during ensemble measurement. We explored this idea by measuring PL of a diluted colloidal suspension of SiNCs in a quartz cuvette under intense mixing. With the same set-up we determined also the PL decay time under various pumping intensities by shifting the delay of a narrow detection window after the pump pulse. The excitation intensity dependence of the integrated PL signal shown in Figure 3b corresponds qualitatively to the results of single SiNC measurements. In addition, we determined the QE of the SiNC suspension by comparing the integrated signal of SiNCs with those of ethanol solution (approximately  $2 \mu\text{mol} \cdot \text{L}^{-1}$ ) of Rhodamine 6G (R6G) under the same conditions. R6G is one of the most studied laser dyes whose QE (in diluted ethanol solutions) is known to be about 90%.<sup>[26]</sup> Under low excitation we found the integrated signal from SiNCs to be below 1/10 of the R6G signal. Therefore the QE of the SiNC suspension is estimated to be around  $7 \pm 3\%$ . The concentration of SiNCs in the suspension (deduced from absorption spectra) is about  $4.5 \times 10^{14} \text{ cm}^{-3}$  and the number of SiNCs in the detected volume is about  $5 \times 10^9$ . The break point of the intensity dependence (Fig. 3b) takes place when about  $2 \times 10^9$  photons per pulse are absorbed in the detected volume (i.e., corresponding – within experimental accuracy – to the absorption rate of one absorbed phonon per nanocrystal per pulse) – this observation confirms the phenomenon of decreasing QE under multiple phonon excitation of a SiNC. The reasons why the value of QE is smaller in ensemble measurements compared to SNS measurements could be most probably an effect of the solvent and/or presence of some “dark” SiNCs that absorb do not emit photons (due to an efficient nonradiative center). The fraction of “dark” nanocrystals is however much lower (<50%) than reported by Credo et al.<sup>[4]</sup> (~97%).

Taking the measured PL decay time  $\tau_{\text{PL}}$  and QE  $\eta$  we can calculate the radiative  $\tau_r$  and nonradiative  $\tau_{\text{nr}}$  lifetimes using the equation

$$\eta = \frac{\tau_{\text{PL}}}{\tau_r} = \frac{1/\tau_r}{1/\tau_r + 1/\tau_{\text{nr}}}$$

As expected, the results show (see Fig. 3b) that the PL decay time is governed by the nonradiative lifetime which shortened with increasing excitation. The radiative lifetime is more than an order of magnitude longer and independent on excitation intensity.

The last step of this discussion should be the microscopic model of the radiative and nonradiative processes in an individual Si nanocrystal (see Fig. 4). After absorption of a photon an electron-hole pair – exciton – is formed in a SiNC. In

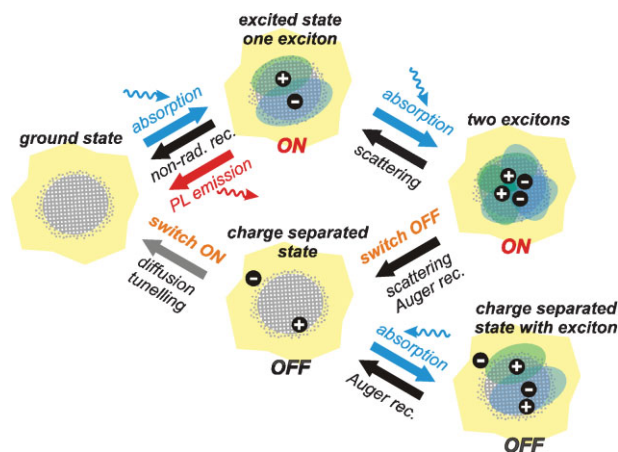


Figure 4. Schematic illustration of processes involved in the radiative and nonradiative recombination of a single Si nanocrystal.

small nanocrystals (diameter below 5 nm), the exciton is strongly confined (Bohr radius of exciton in bulk Si is 4.9 nm). The electron and hole “feel” strongly the amorphous-like interface between the Si core and SiO<sub>2</sub> shell and the related specific vibrations – phonons that take part in recombination processes (influencing the spectral shape). The exciton diffuses in the complex energy landscape and can possibly meet a nonradiative center (e.g., *P<sub>b</sub>* center<sup>[27]</sup>) that is reducing the average QE of radiative recombination. Considering the very slow PL decay typical for measurements in an ensemble of SiNCs (note that here we are not studying the ultrafast recombination phenomena observed under femtosecond excitation<sup>[28]</sup>) and the relatively high QE of the radiative recombination of single SiNC in ON state, there is a high probability of generation of a second exciton during the lifetime of the first one. We suppose that exciton–exciton scattering is the crucial phenomenon in radiative and nonradiative recombination processes of SiNCs. The inelastic scattering induces the nonradiative recombination of one exciton and excitation of the second one. In fact, the same effect can be produced by Auger recombination of an exciton with a third quasiparticle. Here the SiNC is still in the ON state but the QE is reduced. If the exchanged energy is high enough and the energy landscape is favorable, the scattering can lead to a charge separation. In the charge-separated state, the Auger recombination efficiently quenches created excitons, hence causing the NC to become dark until the charges recombine back.

## 4. Conclusions

In conclusions, we have performed studies of individual Si nanocrystals within porous Si grains using both wide-field imaging microspectroscopy and blinking detection by confocal SPC microscopy. These experiments enable us to explain the apparent inconsistency in reported single SiNC spectral shapes and blinking statistics results published by different groups.

The PL properties of single Si nanocrystals are surprisingly insensitive to preparation and treatment conditions. Our analysis shows that only one major (slow) PL center can produce light. At high excitation the excess excitons are gradually quenched by nonradiative recombination. However, the effect of Auger recombination is not as strong as usually anticipated and it seems like nanocrystals may be pumped above one exciton per nanocrystal enabling more intense light generation and possibly population inversion. If the effect of OFF switching is excluded (by considering only the signal from ON periods) the quantum yield is found to be around 0.15 up to a pumping rate of  $2 \times 10^4 \text{ photon} \cdot \text{s}^{-1}$  and then decreases slowly as the 0.7th power of excitation for another three orders of magnitude without clear saturation. These results indicate excellent emission performance of the SiNC/SiO<sub>2</sub> nanostructures that is mainly limited by the persistent OFF switching. In order to exploit maximally, the light-emitting properties of such Si nanostructures the problem of intermittency must be solved. We believe, however, that this can be improved by a proper engineering of the nanocrystal interface and oxide shell as we have indeed observed stable PL from some single nanocrystals without any intermittency effects. The ultimate performance of SiNCs could be also altered for example by interaction with surface plasmons in metallic nanostructures in close proximity of SiNCs,<sup>[29]</sup> by incorporation of SiNCs into different matrices, by surface SiNCs functionalization or in properly interacting closely spaced ensembles of nanocrystals.

The ensemble PL measurements under fast refreshment of the suspension confirm the findings of single SiNC experiments and indicate that the majority of absorbing nanocrystals in the ensemble is able to emit light efficiently. Therefore the previous observations that only a few percent of SiNCs in an ensemble shows detectable light<sup>[4,11]</sup> was most probably a consequence of long persistency of SiNCs in the OFF state.

## 5. Experimental

**Sample Fabrication and Characterization:** Porous silicon layers were prepared by electrochemical etching of *p*-type silicon wafers ((100),  $\sim 0.1 \Omega \text{cm}$ ) in a solution containing hydrofluoric acid HF (50%), pure ethanol (99.9% for UV), and hydrogen peroxide H<sub>2</sub>O<sub>2</sub> (3%). The bath composition, etching time, and current were HF/EtOH/H<sub>2</sub>O<sub>2</sub> = 1:2.46:0.54, 2 h, and 2.3 mA cm<sup>-2</sup>, respectively. Moreover, the freshly prepared PSi layer on the Si wafer was immediately dipped into pure H<sub>2</sub>O<sub>2</sub> (3%) for 5 min in a postetching procedure (to reduce SiNCs dimensions and to obtain – to as large as possible extent – isolated nanocrystals in a SiO<sub>2</sub> matrix). A PSi powder was then obtained by mechanical pulverization of the PSi film from the Si substrate. Colloidal suspensions studied in this work were prepared by pouring ethanol or isopropanol onto the PSi powder and mixing in an ultrasonic bath. Optical microscopical observation shows that the original powder contains many large PSi grains of several  $\mu\text{m}$  or even tens of  $\mu\text{m}$  and sonication is inefficient to break the largest grains to sizes below a  $\mu\text{m}$  [30]. Further size selection is necessary. Here we applied filtering of the supernatant part of sedimented colloidal suspension by membranes with pores of 100 nm (Millex Millipore). This procedure gives a low-concentrated optically clear suspension that may be further diluted and deposited on cleaned substrates. The PSi

grain concentration in the suspension is not known (sedimentation and filtering removes most of the original PSi powder) so the proper dissolution must be found empirically to optimize the density of emitting objects observed in a microscope (see Fig. 1a).

The PSi particles contained in the suspension were characterized with high-resolution transmission electron microscopy (HR-TEM). A drop of the suspension was deposited on a grid with a carbon membrane and imaged in a JEOL JEM-3010 HR-TEM microscope. These observations often show that PSi grains consist of many SiNCs (sometimes almost interconnected and kept together most probably by amorphous silicon oxide) with diameters ranging from about 2 to 5 nm (see inset in Fig. 5).

The initial colloidal suspensions of PSi grains in ethanol exhibit the PL typical of Si nanostructures (Figs. 5a and c) with the two most abundant PL bands often called the F-band and the S-band. The name of the F- and S-bands located in the ultraviolet-blue and yellow-orange-red spectral regions, respectively, comes from their fast (F) and slow (S) PL decay at RT (several nanoseconds and several tens or hundreds of  $\mu\text{s}$ , respectively). In our samples, the S-band is dominant and intentionally shifted to the yellow region (peak around 600 nm) due to small average size (2–3 nm) of SiNCs obtained by additional oxidative activity of H<sub>2</sub>O<sub>2</sub> and relatively low etching current density. In the following, we describe exclusively the properties of the S-band emission. The influence of the F-band is minimized by choosing excitation wavelength around 443 nm (2.8 eV), i.e., inside the F-band.

**Experimental Set-ups and Data Treatment:** PL spectra of single PSi grains have been detected with an imaging microspectroscopy set-up based on an inverted fluorescence microscope (Olympus IX-70) coupled to an imaging spectrometer (Triax 320, Horiba Jobin-Yvon) and a liquid-nitrogen-cooled camera (with a back-thinned CCD chip, Marconi 42–10) attached to the imaging output of the spectrometer. In order to reduce the emission background to a minimum, a drop of the suspension (10  $\mu\text{L}$ ) was deposited directly on a quartz prism (see inset in Fig. 1) and excited by an evanescent field of the laser beam (442 nm line of a He–Cd laser) totally reflected inside the prism. The emitted light was collected by the Olympus UMPlanFl 100 $\times$ /0.95 objective lens and filtered by an edge filter (Semrock RS 442 LP). The image of a sample was created on the entrance slit of the spectrometer and then imaged by a mirror (Fig. 1c) or dispersed with the diffraction grating (see Ref. [31] for more detailed description of the imaging spectroscopy principle). The detection time of PL spectra on the CCD camera were

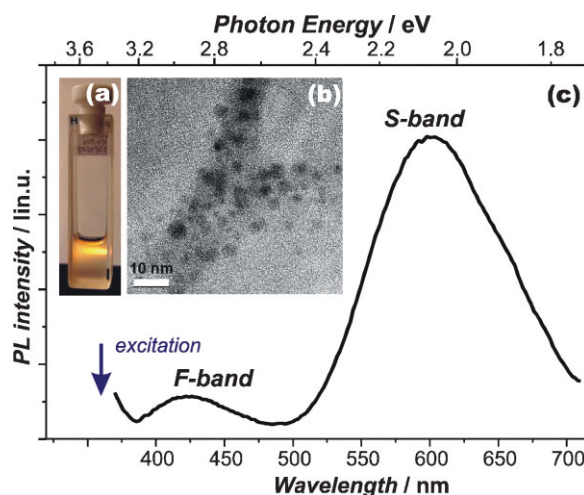


**Figure 5.** Characterization of the initial PSi suspension. a) The photograph of the UV-laser excited cuvette with suspension demonstrating yellow appearance of PL. b) The HR-TEM image of one PSi grain. c) The PL spectrum of a typical “yellow” PSi colloidal suspension (nonfiltered) under UV excitation (a Xe lamp monochromatized at 360 nm).

typically between 10 and 30 min. Spectra of several objects may be obtained simultaneously if their images lie in the region restricted by the entrance slit.

PL blinking was detected with an SPC microscope consisting of the inverted fluorescence microscope Olympus IX-81 coupled to a (Micro Time 200) photon-correlation detection system. The sample was deposited on a cleaned quartz cover slide and observed with the water immersion lens Olympus UPlanS Apochromat 60×/1.2. Excitation was done through the same lens by a blue diode laser (444 nm) used in a continuous-wave regime. The signal was filtered with a long-pass filter, focused on a confocal hole and detected by a pair of avalanche photodiode photon counting (APD-PC) modules (Perkin Elmer SPCM-AQR). The arrival time of all detected photons is recorded and treated numerically after experiments (data from both detectors are taken together).

The ensemble PL QE and decay have been studied by exciting the suspension in a quartz cuvette with the output from a pulsed optical parametric oscillator (PG 122, Ekspla) pumped by a Nd:YAG laser (NL 303, Ekspla). The pumping wavelength, pulse duration, and repetition rate were 443 nm, 5 ns, and 10 Hz, respectively. The emitted light was collected in 90° geometry, imaged on the entrance slit of an imaging spectrometer Triax 320 (Horiba Jobin-Yvon) and detected by an intensified CCD camera (PI-Max, Princeton Instruments). The reference sample was a weak solution of Rhodamine 6G in ethanol (approximately 2 μmol · L<sup>-1</sup>) with an absorption coefficient at the pumping wavelength comparable to the SiNC sample. With the same set-up we determined also the PL decay time under various pumping intensities by shifting the delay of a narrow detection window after the pump pulse.

Received: March 20, 2008

Revised: May 21, 2008

Published online:

- [1] S. Ossicini, L. Pavesi, F. Priolo, *Light Emitting Silicon for Microphotonics*, Springer Tracks in Modern Physics, Vol. 194, Springer Verlag, Berlin, Germany **2003**.
- [2] S. A. Empedocles, R. Neuhauser, K. Shimizu, M. G. Bawendi, *Adv. Mater.* **1999**, *11*, 1243.
- [3] M. D. Mason, G. M. Credo, K. D. Weston, S. K. Buratto, *Phys. Rev. Lett.* **1998**, *80*, 5405.
- [4] G. M. Credo, M. D. Mason, S. K. Buratto, *Appl. Phys. Lett.* **1999**, *74*, 1978.
- [5] M. D. Mason, D. J. Sirbully, P. J. Carson, S. K. Buratto, *J. Chem. Phys.* **2001**, *114*, 8119.
- [6] F. Cichos, J. Martin, Ch. von Borczyskowski, *Phys. Rev. B* **2004**, *70*, 115314.
- [7] F. Cichos, J. Martin, Ch. von Borczyskowski, *J. Lumin.* **2004**, *107*, 160.
- [8] J. Martin, F. Cichos, Ch. von Borczyskowski, *J. Lumin.* **2004**, *108*, 347.
- [9] J. Martin, F. Cichos, F. Huisken, Ch. von Borczyskowski, *Nano Lett.* **2008**, *8*, 656.
- [10] D. S. English, L. E. Pell, Z. Yu, P. F. Barbara, B. A. Korgel, *Nano Lett.* **2002**, *2*, 681.
- [11] J. Valenta, R. Juhasz, J. Linnros, *Appl. Phys. Lett.* **2002**, *80*, 1070.
- [12] J. Valenta, R. Juhasz, J. Linnros, *J. Lumin.* **2002**, *98*, 15.
- [13] I. Sychugov, R. Juhasz, J. Valenta, J. Linnros, *Phys. Rev. Lett.* **2005**, *94*, 087405.
- [14] I. Sychugov, R. Juhasz, J. Linnros, J. Valenta, *Phys. Rev. B* **2005**, *71*, 115331.
- [15] I. Sychugov, R. Juhasz, A. Galeckas, J. Valenta, J. Linnros, *Opt. Mater.* **2005**, *27*, 973.
- [16] M. Lippitz, F. Kulzer, M. Orrit, *Chem. Phys. Chem.* **2005**, *6*, 770.
- [17] A. L. Efros, M. Rosen, *Phys. Rev. Lett.* **1997**, *78*, 1110.
- [18] K. T. Shimizu, R. G. Neuhauser, C. A. Leatherdale, S. A. Empedocles, W. K. Woo, M. G. Bawendi, *Phys. Rev. B* **2001**, *63*, 205316.
- [19] J. Tang, R. A. Marcus, *Phys. Rev. Lett.* **2005**, *95*, 107401.
- [20] P. A. Frantsuzov, R. A. Marcus, *Phys. Rev. B* **2005**, *72*, 155321.
- [21] J. Tang, R. A. Marcus, *J. Chem. Phys.* **2006**, *125*, 044703.
- [22] J. Tang, *J. Chem. Phys.* **2007**, *127*, 111105.
- [23] D. Kovalev, H. Heckler, G. Polisski, F. Koch, *Phys. Status Solidi B* **1999**, *215*, 871.
- [24] D. Kovalev, J. Diener, H. Heckler, G. Polisski, N. Kunzner, F. Koch, *Phys. Rev. B* **2000**, *61*, 4485.
- [25] C. Delerue, G. Allan, C. Reynaud, O. Guillois, G. Ledoux, F. Huisken, *Phys. Rev. B* **2006**, *73*, 235318.
- [26] L. S. Rohwer, J. E. Martin, *J. Lumin.* **2005**, *115*, 77.
- [27] P. Pellegrino, B. Garrido, C. García, R. Ferré, J. A. Moreno, J. R. Morante, *Phys. E* **2003**, *16*, 424.
- [28] F. Trojánek, K. Neudert, P. Malý, K. Dohnalová, I. Pelant, *J. Appl. Phys.* **2006**, *99*, 116108.
- [29] J. S. Biteen, D. Pacifici, N. S. Lewis, H. A. Atwater, *Nano Lett.* **2005**, *5*, 1768.
- [30] J. Valenta, P. Janda, K. Dohnalová, D. Nižňanský, F. Vácha, J. Linnros, *Opt. Mater.* **2005**, *27*, 1046.
- [31] J. Valenta, J. Linnros, R. Juhasz, F. Cichos, J. Martin, in *Towards the First Silicon Laser* (Eds: L. Pavesi, S. Gaponenko, L. Dal Negro), Kluwer Academic, Dordrecht, the Netherlands **2003**, p. 89.